Analyzing the Differences of Initiation Strength Between Embedded Crack and Penetrating Crack

Han BAO(1,2), Faquan WU(1), Jinyuan CHANG(3), Ning LIANG(1,2)

(1) Key Laboratory of Shale Gas and Geoengineering, Institute of Geology and Geophysics, Chinese Academy of Sciences, Beijing 100029, China
E-mail: baohangeo@163.com
(2) University of Chinese Academy of Sciences, Beijing 100049, China
(3) College of Civil Engineering, Shaoxing University, Shaoxing Zhejiang, 312000, China

Abstract

Based on the maximum energy release rate criterion of fracture mechanics, we deduced and compared the initiation strength expressions about embedded crack and penetrating crack under three-dimensional condition. Results showed that the initiation strength of both two types of cracks could be described by equal-slope linear function with confining pressure as independent variable, and the initiation strength of embedded crack was larger than that of penetrating crack. The relative differences of initiation strength between the two types of cracks usually should not be ignored, they were related with confining pressure and the parameters of rock and crack. When the dip angle of crack was $\frac{\pi}{4}+\frac{\varphi_w}{2}$ (φ_w is the friction angle of crack), the differences would be minimum. And the differences tended to be stable when the radius exceeded a certain value. Generally speaking, the differences of initiation strength would be large for good quality rock or stable crack.

Keywords: embedded crack, penetrating crack, initiation strength

1. Introduction

Cracks (joints) have remarkable effects on the mechanical properties of rock mass. Many studies have been done on the mechanical behavior of cracks, in which crack initiation strength is always a hot spot. When studying crack propagation mechanism of brittle materials, three important breakage initiation criteria are usually used, i.e., the maximum tangential stress criterion (σ-criterion), the maximum energy release rate criterion (G-criterion) and the minimum energy density criterion (S-criterion). Cracks have multiple propagation modes under compressive stress. In general, only mode I and mode II cracks (i.e., tensile cracks and shear cracks) would be observed originating from the original tips of pre-existing cracks (Lajtai, 1974; Bobet and Einstein, 1998). However, mode III cracks (i.e., tear cracks) could also be observed in some experiments (Wong et al., 2006). Many factors might have effects on the crack initiation strength, including crack attitude (Gong et al., 2005), crack length, dip angle, sample size (Wong et al., 2002), seepage pressure (Li et al., 2012), microstructure (Hatzor et al., 1997), rock type, mineral particle size, cementing quality and schistosity (Zhang et al., 2011). Many studies also showed that crack initiation strength of rock mass was much lower than peak strength under compressive stress (Nicksiar and Martin, 2014; Cai et al., 2004). Thus, it is of great significance to take crack initiation strength into account for the stability of engineering.

In fact, several types of cracks exist in engineering rock mass, in which embedded and penetrating cracks are two common types. Embedded cracks are widespread in rock mass, while penetrating

cracks are often found in bedded rock mass, high degree jointed rock mass, and shallow free faces of slopes, tunnels and underground caverns. Though a large amount of studies have been done on the crack mechanical behaviors (Haeri et al., 2013; Wong et al., 2002), we have rarely discussed embedded crack and penetrating crack together, their differences on initiation strength have also been rarely studied. Sometimes, we even didn't make a distinction between embedded crack and penetrating crack in studies or applications, such as when generalizing three-dimensional situations into two-dimensional models. Due to the significant influences of initiation strength on engineering stability, it is worthy to study the differences of initiation strength between embedded crack and penetrating crack.

Therefore, on the basis of the maximum energy release rate criterion (G-criterion), we deduced expressions of crack initiation strength under composite breakage. Depending on the deduced expressions, we then analyzed the differences of initiation strength between embedded crack and penetrating crack and their influencing factors as well. Our study was supposed to make a positive contribution to the cognition of mechanical behaviors of different types of cracks.

2. Conceptual models of cracked rock mass

In three-dimensional space, we established conceptual models of rock mass with embedded crack (Fig. 1a) and penetrating crack (Fig. 1b) as follows:

In three-dimensional Cartesian coordinate system, the negative direction of *X* axes points to 0° and the positive direction of *Y* axes points to 90°. Maximum principal stress (σ_1), medium principal stress (σ_2) and minimum principal stress (σ_3) are in the directions of *Z* axes, *X* axes and *Y* axes, respectively. It is noted that we set compressive stress to be positive. α, β, φ_w, c_w are the dip direction angle, dip angle, fraction angle and cohesion of a single crack, respectively. φ_0, c_0 and ν are internal friction angle, cohesion and Poisson's ratio of rock, respectively. The radius of embedded penny-shape crack is a. The length of penetrating crack is $2a$ (we treated a as the radius of penetrating crack), the crack tends to the same direction of crack length, B is the penetrating thickness of crack in rock mass.

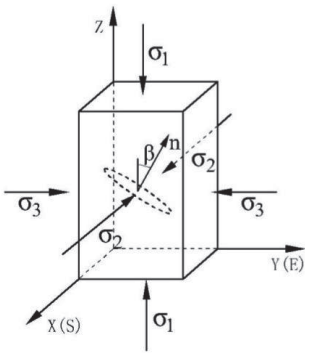

a. Embedded crack model

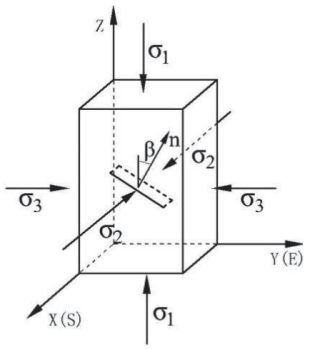

b. Penetrating crack model

Fig.1 Rock mass models with single crack

Thus, the normal direction cosine of the cracks could be obtained as follows:

$$\begin{aligned} n_1 &= -\cos\alpha\sin\beta \\ n_2 &= \sin\alpha\sin\beta \\ n_3 &= \cos\beta \end{aligned} \tag{1}$$

We define the surplus shear stress on the cracks as τ. By assuming δ as the angle between *X* axes and τ, and θ as the angle between X axes and edge point of cracks (Fig. 2), the value of τ can be calculated according to Eq. (2) .

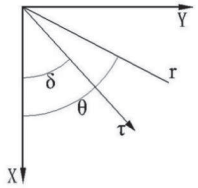

Fig.2 Shear stress direction on crack

$$\tau = \begin{cases} t - s & t \geq s \\ 0 & t < s \end{cases} \tag{2}$$

where t is the shear stress on the cracks and s is the shear strength on the cracks. t and s can be calculated as follows:

$$\begin{aligned} t &= \sqrt{\sigma_{11}^2 n_3^2 + \sigma_{22}^2 n_1^2 + \sigma_{33}^2 n_2^2 - (\sigma_{11} n_3^2 + \sigma_{22} n_1^2 + \sigma_{33} n_2^2)^2} \\ s &= (\sigma_1 n_3^2 + \sigma_2 n_1^2 + \sigma_3 n_2^2) \tan \varphi_w \end{aligned} \quad (3)$$

3. Initiation strength criteria of the two types of cracks

3.1 Deduction of initiation strength criteria

Three modes of stress intensity factor (SIF) of embedded crack and penetrating crack can be obtained from reference (Li et al., 2010) under three-dimensional stress condition showed in Fig.1. Noting that the mode I crack is tensile cracks which reflects the reaction of tensile stress, a parameter k is introduced to reflect stress state on the normal direction of crack. If the stress is tensile stress, $k = 1$, or $k = 0$.

The SIFs of embedded crack are shown as follows:

$$\begin{aligned} K_{\mathrm{I}e} &= \frac{2}{\sqrt{\pi}} k \sigma_n \sqrt{a} \\ K_{\mathrm{II}e} &= \frac{4\tau\sqrt{a}}{(2-\nu)\sqrt{\pi}} \cos(\theta - \delta) \\ K_{\mathrm{III}e} &= -\frac{4(1-\nu)\tau\sqrt{a}}{(2-\nu)\sqrt{\pi}} \sin(\theta - \delta) \end{aligned} \quad (4)$$

where σ_n is the normal stress of crack. The conceptual model with penetrating crack can be generalized to a two-dimension model, so the SIF of penetrating crack are expressed as Eq. (5) under the condition of plane strain.

$$\begin{aligned} K_{\mathrm{I}p} &= k \sigma_n \sqrt{\pi a} \\ K_{\mathrm{II}p} &= \tau_a \sqrt{\pi a} \\ K_{\mathrm{III}p} &= \tau_B \sqrt{\pi a} \end{aligned} \quad (5)$$

Where τ_a and τ_B are components of τ along length and penetrating direction of crack, respectively.

Assuming the rock is linear elasticity material, we can get the strain energy release rate of crack under three failure modes based on G-criterion. The three strain energy release rate of embedded crack are listed in Eq. (6) (Wu, 1993).

$$\begin{aligned} G_{\mathrm{I}e} &= \frac{1-\nu^2}{E} K_{\mathrm{I}e}{}^2 \\ G_{\mathrm{II}e} &= \frac{(1-\nu^2)(2-\nu)}{2E} K_{\mathrm{II}e}{}^2 \\ G_{\mathrm{III}e} &= \frac{(1+\nu)(2-\nu)}{2E(1-\nu)} K_{\mathrm{III}e}{}^2 \end{aligned} \quad (6)$$

Thus, the strain energy release rate of composite mode crack is

$$\begin{aligned} G &= G_{\mathrm{I}e} + G_{\mathrm{II}e} + G_{\mathrm{III}e} \\ &= \frac{1-\nu^2}{E} [K_{\mathrm{I}e}^2 + \frac{2-\nu}{2} K_{\mathrm{II}e}^2 + \frac{2-\nu}{2(1-\nu)^2} K_{\mathrm{III}e}^2] \end{aligned} \quad (7)$$

The three strain energy release rate of penetrating crack are

$$\begin{aligned} G_{\mathrm{I}p} &= \frac{1-\nu^2}{E} K_{\mathrm{I}p}^2 \\ G_{\mathrm{II}p} &= \frac{1-\nu^2}{E} K_{\mathrm{II}p}^2 \\ G_{\mathrm{III}p} &= \frac{1+\nu}{E} K_{\mathrm{III}p}^2 \end{aligned} \quad (8)$$

Then the strain energy release rate of composite mode crack can be written as

$$\begin{aligned} G &= G_{\mathrm{I}p} + G_{\mathrm{II}p} + G_{\mathrm{III}p} \\ &= \frac{1-\nu^2}{E} K_{\mathrm{I}p}^2 + \frac{1-\nu^2}{E} K_{\mathrm{II}p}^2 + \frac{1+\nu}{E} K_{\mathrm{III}p}^2 \end{aligned} \quad (9)$$

G-criterion states that if energy release rate is equal to consumed surface energy, the system will be in a critical state, i.e., G reaches the critical value of G_{Jc}, and the crack starts propagation. Assuming the consumed surface energy of composite breakage is equal to mode I propagation, namely new equal superficial area, then we can get Eq. (10).

$$G = G_{\mathrm{Ic}} = \frac{1-\nu^2}{E} K_{\mathrm{Ic}}^2 \tag{10}$$

For embedded crack, Eq. (10) can be derived as

$$K_{\mathrm{Ic}}^2 = K_{\mathrm{Ie}}^2 + \frac{2-\nu}{2} K_{\mathrm{IIe}}^2 + \frac{2-\nu}{2(1-\nu)^2} K_{\mathrm{IIIe}}^2 \tag{11}$$

Substituting Eq. (4) into Eq. (11), we can have

$$(k\sigma_n^2 + \frac{2}{2-\nu}\tau^2)\frac{4}{\pi}a = K_{\mathrm{Ic}}^2 \tag{12}$$

For penetrating crack, Eq. (13) and Eq. (14) are deduced with the same method mentioned above.

$$K_{\mathrm{Ic}}^2 = K_{\mathrm{Ip}}^2 + K_{\mathrm{IIp}}^2 + \frac{1}{1-\nu} K_{\mathrm{IIIp}}^2 \tag{13}$$

$$(k\sigma_n^2 + \tau_a^2 + \frac{\tau_B^2}{1-\nu})\pi a = K_{\mathrm{Ic}}^2 \tag{14}$$

Assuming rock mass is under compressive stress with a constant confining pressure, we can have $\sigma_2 = \sigma_3$ and $k = 0$. For penetrating crack, $\tau_a = \tau$ and $\tau_B = 0$. Substituting Eq. (1), Eq. (2) and Eq. (3) into Eq. (12) and Eq. (14), we can get the crack initiation strength criteria of embedded crack and penetrating crack as follows.

For embedded crack:

$$\sigma_{1e} = \frac{\sin(2\beta-\varphi_w)+\sin\varphi_w}{\sin(2\beta-\varphi_w)-\sin\varphi_w}\sigma_3 + \frac{2(\mathrm{c}_w + K_{\mathrm{Ic}}\sqrt{\frac{\pi(2-\nu)}{8a}})\cos\varphi_w}{\sin(2\beta-\varphi_w)-\sin\varphi_w} \tag{15}$$

For penetrating crack:

$$\sigma_{1p} = \frac{\sin(2\beta-\varphi_w)+\sin\varphi_w}{\sin(2\beta-\varphi_w)-\sin\varphi_w}\sigma_3 + \frac{2(\mathrm{c}_w + K_{\mathrm{Ic}}\sqrt{\frac{1}{\pi a}})\cos\varphi_w}{\sin(2\beta-\varphi_w)-\sin\varphi_w} \tag{16}$$

Eq. (15) and Eq. (16) indicate that crack initiation strength is not only related to dip angle, length, friction angle and cohesion of crack, but also related to mode I fracture toughness and Poisson's ratio of rock. Additionally, the crack initiation strength is also positively related to confining pressure and varies with dip angle. Through derivation we can get the minimum values of Eq. (15) and Eq. (16) both when $\beta = \frac{\pi}{4} + \frac{\varphi_w}{2}$. If the crack is continuous, there is no fracture mechanical effect on the crack, then $K_{\mathrm{Ic}} = 0$. Thus Eq. (15) and Eq. (16) can be transformed into Mohr-Coulomb criterion.

3.2 Verification of initiation strength criteria

We verified the reasonability of initiation strength criteria using a series of physical model tests with penetrating crack conducted by Xiao et al. (2012). Taking the deep buried marble at Jinping II hydropower station as original sample, Xiao et al. (2012) made the physical model samples with standard size of ϕ50 mm×100 mm using high strength silica powder mortar, in which two groups of model samples had single pre-crack with 13mm length and 19mm length, respectively, and the dip angles of the pre-cracks were all 60°.

Table 1 shows the related indices about marble and physical model. Two groups of samples were compressed to failure under confining pressure of 7, 14 and 21 MPa, and the values of peak strength were recorded. We used Eq. (16) to calculate the initiation strength and then compared it to the peak strength (Table 2). The value of K_{Ic} was calculated following Zhang (2002), i.e., $K_{\mathrm{Ic}} = \sigma_t / 6.88$.

Table 1 Physical-mechanical indices of silicon powder mortar model samples and marble original sample (Data source: Xiao et al. (2012))

Material	$\rho/(g\cdot cm^{-3})$	E/GPa	ν	σ_c/MPa	σ_t/MPa	c_0/MPa	φ_0/°	φ_w/°
Physical model	2.207	14.19	0.12	70.12	2.16	20.73	35.0	30
Marble	2.700	25.20	0.14	199.20	5.57	61.13	35.8	--

*ρ is material density; E is elasticity modulus; ν is Poisson's ratio; σ_c is uniaxial compressive strength; σ_t is uniaxial tensile strength; c_0 is cohesion of material; φ_0 is internal friction angle of material; φ_w is friction angle of crack.

Table 2 Strength analysis of physical models

Samples	Crack length/mm	Peak strength/MPa	Confining pressure/MPa	Initiation strength/MPa	Initiation strength/peak strength
Group1	13	89.50	7	28.61	0.319
	13	99.86	14	49.61	0.497
	13	114.58	21	70.61	0.616
Group2	39	53.50	7	25.39	0.475
	39	82.08	14	46.39	0.565
	39	109.59	21	67.39	0.615

Results show that the initiation strength increases with the increase of confining pressure but decreases with the increase of crack length. And the ratio of initiation strength to peak strength increases with both confining pressure and crack length, with values ranging from 0.32 to 0.62 (Table 2). The ratio values obtained in Liu et al. (2012) and Martin and Chandler (1994) for marble at Jinping II hydropower station and brittle rock, respectively, are around 0.4 to 0.5, which indicate that our results are similar to the existing studies. However, the ratio values of rock mass with macrocrack have larger range than that of intact rock. The reason is that macrocrack is easier to produce stress concentration than microcrack so that shows smaller values in low confining pressure. But when the confining pressure increasing, the structure control become weak and the strength of cracked rock mass increases so rapidly that make the ratio values increase too. Additionally, the physical model material may convert from brittleness to ductility under the condition of high confining pressure, while the criteria derived in this paper cannot be applied to ductile material, so we can get higher ratio values in high confining pressure.

4. Comparison of the initiation strength between embedded crack and penetrating crack

We define R_σ as the initiation strength ratio between embedded crack and penetrating crack to express the relative differences. Thus, R_σ can be derived form Eq. (15) and Eq. (16) as:

$$R_\sigma = \frac{\sigma_{1e}}{\sigma_{1p}} = 1 + \frac{K_{\mathrm{Ic}}\left(\sqrt{\frac{\pi(2-\nu)}{8a}} - \sqrt{\frac{1}{\pi a}}\right)}{(\sin\beta\cos\beta + \sin^2\beta\tan\varphi_w)\sigma_3 + c_w + K_{\mathrm{Ic}}\sqrt{\frac{1}{\pi a}}} \tag{17}$$

Obviously, the initiation strength of embedded crack is higher than that of penetrating crack, so $R_\sigma \geq 1$, where R_σ is related with rock mass mechanics properties, geometry and mechanics of crack and confining pressure. In order to figure out the influences of factors on R_σ, we adopt single factor analysis method to study the change of

R_σ under different confining pressure. The parameters of rock are based on the parameters of marble in Table 1 and the parameters of Jinping marble joints (cracks) are based on Chen et al. (2008), in which radius $a = 0.382$ m, dip angle $\beta = 40^\circ$, cohesion $c_w = 0.07$ MPa, and friction angle $\varphi_w = 30.44^\circ$. The results are showed in Fig. 3.

The variation ranges of factors in Fig. 3 are consistent with the principle of rock mass mechanics and can reflect the real varying patterns of R_σ. Results show that R_σ is in negative but weak correlation with cohesion, friction angle and Poisson's ratio (Fig. 3b, 3d and 3f), i.e., R_σ slowly decreases with the increase of these factors. However, with the increase of radius, R_σ decreases rapidly at first and then become stable gradually (Fig. 3a), which demonstrates that the increase of radius could efficiently reduce the differences of initiation strength between the two types of cracks. Especially, when radius is over some certain limit which is not affected by confining pressure, R_σ tends to be stable. The certain value in this case is about 0.5 m. As to K_{Ic}, R_σ is positively correlated with K_{Ic} and increases rapidly with the increase of K_{Ic} (Fig. 3e). In Fig. 3c, R_σ decreases firstly and then increases with the increase of dip angle, with the minimum value at $\beta = \frac{\pi}{4} + \frac{\varphi_w}{2}$. Fig. 3 indicates that confining pressure has significant effects on R_σ, and R_σ decreases gradually and tends to be 1 with the increase of confining pressure.

Based on the discussion above, we can conclude that there are differences between the initiation strength of embedded crack and penetrating crack, the differences are influenced by confining pressure and parameters of rock and crack. In some cases, the differences maybe reduce to elimination. Therefore,

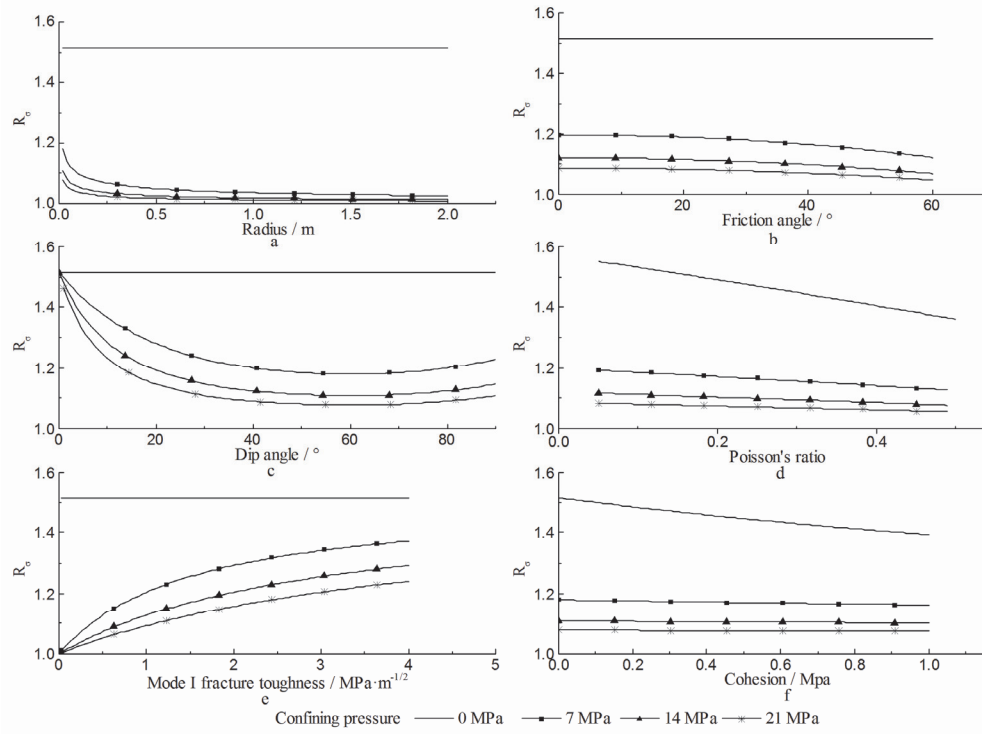

Fig.3 Relationship between R_σ and parameters of rock mass under different confining pressure

whether to distinguish the differences between the embedded crack and penetrating crack in practice depends on properties of rock and crack. In the case of Jingping marble, the value of R_σ we get is 1.2, which indicates that the differences between embedded crack and penetrating crack at Jingping II hydropower station should be considered.

When excluding confining pressure, the ratio R_σ under the condition of uniaxial compression is:

$$R_\sigma = \frac{\sigma_{u1e}}{\sigma_{u1p}} = 1 + \frac{K_{\mathrm{Ic}}(\sqrt{\pi^2(2-\nu)/8}-1)}{K_{\mathrm{Ic}} + c_w\sqrt{\pi a}} \qquad (18)$$

Where σ_{u1e} and σ_{u1p} are initiation strength of embedded and penetrating cracks under uniaxial stress, respectively. Eq. (18) reveals that, under the condition of uniaxial compression, the relative differences between embedded crack and penetrating crack are independent of dip angle and friction angle of crack. The values of R_σ are usually large as Fig. 3 showing. Hence embedded crack and penetrating crack should be treated specifically under the condition of uniaxial compression.

We note that the cohesion of crack is usually small and even negligible. Thus, when $c_w = 0$, the ratio $R_\sigma = \frac{\sigma_{u1e}}{\sigma_{u1p}} = \sqrt{\frac{\pi^2(2-\nu)}{8}}$. Here R_σ is only related with Poisson's ratio and ranges from 1.36 to 1.57 depending on the value of ν.

In general, R_σ will be large with a large K_{Ic} and a small Poisson's ratio, which means good quality rock. Also, when excluding effects of friction angle, R_σ will be large with a small radius, dip angle and cohesion of crack, which means stable structure plane. Therefore, the differences will be large when rock material is good and structure plane is relatively stable.

5. Application condition

Crack types influence the strength of rock mass. In practical applications, we usually regard natural crack as embedded penny-shape. In fact, penetrating cracks are often found in nature because of joints intersection, especially in bedded rock mass. In addition, human activities can lead to new cracks generation, which may help cracks penetrate in one dimension. For instance, slope excavation can generate many tensile cracks paralleling to slope surface, the phenomenon observed in Xiaowan hydropower station is a typical example (Wu et al., 2009). In deep rock mass engineering, zonal disintegration is another phenomenon influenced by human activity which may also transform crack type (Qian and Li, 2008). Therefore, we need to distinguish rock types carefully and pay more attention on the selection of expressions for initiation strength calculation. Crack type is related to rock mass stability, we may get lager safety factors if we use wrong expressions, because the stability of embedded crack may 20% higher than penetrating crack as Jinping marble shows.

6. Conclusion

In this paper, based on the energy criterion of fracture mechanics, we deduced the initiation strength criteria of embedded crack and penetrating crack under three-dimensional stress and obtained the following results by comparing the two criteria.

1. The initiation strength of embedded crack is larger than that of penetrating crack. The initiation strength of embedded crack and penetrating crack can be both expressed by equal-slope linear function with confining pressure as independent variable, and they both have the minimum values when $\beta = \frac{\pi}{4} + \frac{\varphi_w}{2}$.

2. Under a condition of three-dimensional stress, the relative differences of initiation strength between embedded crack and penetrating crack decrease with the increase of confining pressure, and are in positive correlation with mode I fracture toughness of rock but in negative correlation with radius, dip angle, cohesion, friction angle of crack, and Poisson's ratio of rock. Generally speaking, the differences will be large for good quality rock or stable crack.

3. The relative differences of initiation strength

between embedded crack and penetrating crack will be minimum when $\beta=\frac{\pi}{4}+\frac{\varphi_w}{2}$, and tends to be stable when radius exceeds a certain value.

Acknowledgements

This work was financially supported by Key program of National Natural Science Foundation of China (Grant NO. 41030749).

References

Bobet, A., Einstein, H. H. (1998): Numerical modeling of fracture coalescence in a model rock material. International Journal of Fracture, 92(3), 221-252.

Cai, M., Kaiser, P. K., Tasaka, Y., Maejima, T., Morioka, H., Minami, M. (2004): Generalized crack initiation and crack damage stress thresholds of brittle rock masses near underground excavations. International Journal of Rock Mechanics and Mining Sciences, 41(5), 833-847.

Chen, W., Yang, J., Zou, X., ZHOU, C. (2008): Research on macromechanical parameters of fractured rock masses. Chinese Journal of Rock Mechanics and Engineering, 27(8), 1569-1575.

Gong, Q. M., Zhao, J., Jiao, Y. Y. (2005): Numerical modeling of the effects of joint orientation on rock fragmentation by TBM cutters. Tunneling and underground space technology, 20(2), 183-191.

Haeri, H., Shahriar, K., Marji, M. F., Moarefvand, P. (2015): A coupled numerical–experimental study of the breakage process of brittle substances. Arabian Journal of Geosciences, 8(2):809-825.

Hatzor, Y. H., Zur, A., Mimran, Y. (1997): Microstructure effects on microcracking and brittle failure of dolomites. Tectonophysics, 281(3), 141-161.

Lajtai, E. Z. (1974): Brittle fracture in compression. International Journal of Fracture, 10(4), 525-536.

Li, S. Y., He, T. M., Yin, X. C. (2010): Introduction of rock fracture mechanics. China Science and Technology University Press, Hefei.

Liu, N., Zhang, C., Chu, W. (2012): Fracture characteristics and damage evolution law of Jinping deep marble. Chinese Journal of Rock Mechanics and Engineering, 31(8),1006-1013.

Li, X. B., HE, X. Q., CHEN, H. J. (2012): Crack initiation characteristics of opening-mode crack embedded in rock-like material under seepage pressure [J]. Chinese Journal of Rock Mechanics and Engineering, 31(7), 1317-1324.

Martin, C. D., Chandler, N. A. (1994, December): The progressive fracture of Lac du Bonnet granite. In International Journal of Rock Mechanics and Mining Sciences & Geomechanics Abstracts (Vol. 31, No. 6, pp. 643-659). Pergamon.

Nicksiar, M., Martin, C. D. (2014): Factors Affecting Crack Initiation in Low Porosity Crystalline Rocks. Rock mechanics and rock engineering, 47(4), 1165-1181.

Qian, Q. H., Li, S. C. (2008): A review of research on zonal disintegration phenomenon in deep rock mass engineering. Chinese Journal of Rock Mechanics and Engineering, 27(6),1278-1284.

Wong, R. H. C., Tang, C. A., Chau, K. T., Lin, P. (2002): Splitting failure in brittle rocks containing pre-existing flaws under uniaxial compression. Engineering Fracture Mechanics, 69(17), 1853-1871.

Wong, R. H., Guo, Y. S. H., Li, L. Y., Chau, K. T., Zhu, W. S., Li, S. C. (2006): Anti-wing crack growth from surface flaw in real rock under uniaxial compression. In Fracture of Nano and Engineering Materials and Structures (pp. 825-826). Springer Netherlands.

Wu, F. Q. (1993): Principles of statistical mechanics of rock masses. China University of Geosciences Press, Wuhan.

Wu, F. Q, Liu, T., Liu, J. Y, Tang, X. L. (2009): Excavation unloading destruction phenomena in rock dam foundations. Bulletin of Engineering Geology and the Environment, 68(2), 257-262.

Xiao, T. L., Li, X. P, Jia, S. P. (2012): Triaxial test research and mechanical analysis based on structure surface effect of the deep rock mass with single fissure. Chinese Journal of Rock Mechanics and engineering, 31(8), 1666-1673.

Zhang, X. P., Wang, S. J., Han, G. Y., Zhang, B. (2011): Crack propagation study of rock based on uniaxial compressive test—a case study of schistose rock. Chinese Journal of Rock Mechanics & Engineering, 30(9), 1772-1781.

Zhang, Z. X. (2002): An empirical relation between mode I fracture toughness and the tensile strength of rock. International Journal of Rock Mechanics and Mining Sciences, 39(3), 401-406.